(≤0.5 ml) of sea water were analysed by flow cytometry[29] using a Becton Dickinson FACSort. As population abundance is inversely related to cell size, detection of phytoplankton in the small aliquots was usually limited to cells that were abundant, namely the picophytoplankton (<2 μm) and nanophytoplankton (2–20 μm). The microphytoplankton (>20 μm) were not included in our measurements. This limitation is discussed elsewhere[30]. Although the microphytoplankton contribute significantly to total photoautotrophic biomass at various times and places, they were seldom significant on a numerical basis. Cytometric forward light scatter was calibrated using synthetic microspheres[29] and therefore cannot be assumed to measure accurately the size of phytoplankton cells[28]. However, the approximate positions of 2 μm and 10 μm on the light scatter scale were confirmed by flow cytometric analysis of the phytoplankton assemblage after physical size fractionation using Nuclepore polycarbonate membranes.

Received 23 May; accepted 11 July 2002; doi:10.1038/nature00994.

1. Longhurst, A. *Ecological Geography of the Sea* (Academic, San Diego, 1998).
2. Cole, J., Lovett, G. & Findlay S. (eds) *Comparative Analyses of Ecosystems: Patterns, Mechanisms, and Theories* (Springer, New York, 1991).
3. Gasol, J. M. & Duarte, C. M. Comparative analyses in aquatic microbial ecology: how far do they go? *FEMS Microb. Ecol.* **31,** 99–106 (2000).
4. Li, W. K. W. Annual average abundance of heterotrophic bacteria and *Synechococcus* in surface ocean waters. *Limnol. Oceanogr.* **42,** 1746–1753 (1998).
5. Brown, J. H. *Macroecology* (Univ. Chicago Press, Chicago, 1995).
6. Peters, R. H. *The Ecological Implications of Body Size* (Cambridge Univ. Press, Cambridge, 1983).
7. Brown, J. H. & West, G. B. (eds) *Scaling in Biology* (Oxford Univ. Press, New York, 2000).
8. Li, W. K. W. Cytometric diversity in marine ultraphytoplankton. *Limnol. Oceanogr.* **42,** 874–880 (1997).
9. Sommer, U., Padisák, J., Reynolds, C. S. & Juhász-Nagy, P. Hutchinson's heritage: the diversity-disturbance relationship in phytoplankton. *Hydrobiologia* **249,** 1–7 (1993).
10. Li, W. K. W. & Harrison, W. G. Chlorophyll, bacteria and picophytoplankton in ecological provinces of the North Atlantic. *Deep-Sea Res. II* **48,** 2271–2293 (2001).
11. Chisholm, S. W. in *Primary Productivity and Biogeochemical Cycles in the Sea* (eds Falkowski, P. G. & Woodhead, A. D.) 213–237 (Plenum, New York, 1992).
12. Hill, M. O. Diversity and evenness: a unifying notation and its consequences. *Ecology* **54,** 427–432 (1973).
13. Legendre, P. & Legendre, L. *Numerical Ecology*, 2nd edn (Elsevier, Amsterdam, 1998).
14. Yentsch, C. S. & Phinney, D. A. A bridge between ocean optics and microbial ecology. *Limnol. Oceanogr.* **34,** 1694–1705 (1989).
15. Ciotti, Á. M., Lewis, M. R. & Cullen, J. J. Assessment of the relationships between dominant cell size in natural phytoplankton communities and the spectral shape of the absorption coefficient. *Limnol. Oceanogr.* **47,** 404–417 (2002).
16. Damuth, J. D. Common rules for animals and plants. *Nature* **395,** 115–116 (1998).
17. Enquist, B. J., Brown, J. H. & West, G. B. Allometric scaling of plant energetics and population density. *Nature* **395,** 163–165 (1998).
18. Laws, E. A. & Archie, J. W. Appropriate use of regression analysis in marine biology. *Mar. Biol.* **65,** 13–16 (1981).
19. Montagnes, D. J. S., Berges, J. A., Harrison, P. J. & Taylor, F. J. R. Estimating carbon, nitrogen, protein, and chlorophyll *a* from volume in marine phytoplankton. *Limnol. Oceanogr.* **39,** 1044–1060 (1994).
20. Agustí, S. & Kalff, J. The influence of growth conditions on the size dependence of maximal algal density and biomass. *Limnol. Oceanogr.* **34,** 1104–1108 (1989).
21. Belgrano, A., Allen, A. P., Enquist, B. J. & Gillooly, J. F. Allometric scaling of maximum population density: a common rule for marine phytoplankton and terrestrial plants. *Ecol. Lett.* (in the press).
22. Cullen, J. J., Franks, P. J. S., Karl, D. M. & Longhurst, A. in *Biological–Physical Interactions in the Sea* (eds Robinson, A. R., McCarthy, J. J. & Rothschild, B. J.) *The Sea* **Vol. 12 297–336 (Wiley,** New York, 2002).
23. Rodríguez, J. *et al.* Mesoscale vertical motion and the size structure of phytoplankton in the ocean. *Nature* **410,** 360–363 (2001).
24. Rodríguez, J. Some comments on the size-based structural analysis of the pelagic ecosystem. *Sci. Mar.* **58,** 1–10 (1994).
25. Cyr, H. in *Scaling in Biology* (eds Brown, J. H. & West, G. B.) 267–295 (Oxford Univ. Press, New York, 2000).
26. Connell, J. Diversity in tropical rain forests and coral reefs. *Science* **199,** 1304–1310 (1978).
27. Reynolds, C. S. *Vegetation Processes in the Pelagic: a Model for Ecosystem Theory* (Ecology Institute, Oldendorf/Luhe, 1997).
28. Cavender-Bares, K. K., Rinaldo, A. & Chisholm, S. W. Microbial size spectra from natural and nutrient enriched ecosystems. *Limnol. Oceanogr.* **46,** 778–789 (2001).
29. Li, W. K. W. Composition of ultraphytoplankton in the central North Atlantic. *Mar. Ecol. Prog. Ser.* **122,** 1–8 (1995).
30. Li, W. K. W. & Dickie, P. M. Monitoring phytoplankton, bacterioplankton, and virioplankton in a coastal inlet (Bedford Basin) by flow cytometry. *Cytometry* **44,** 236–246 (2001).

Acknowledgements

I thank all seagoing staff of the Biological Oceanography Section at Bedford Institute of Oceanography for collecting samples. I am grateful to C. Reynolds, G. Harrison, T. Platt and P. Falkowski for reading the manuscript. I also thank A. Belgrano for sharing his knowledge and pre-publication work on allometry with me. Financial support was provided by DFO Strategic Science Fund in the Ocean Climate Program, and the Interdepartmental Panel on Energy R&D.

Competing interests statement

The author declares that he has no competing financial interests.

Correspondence and requests for materials should be addressed to W.K.W.L. (e-mail: Lib@mar.dfo-mpo.gc.ca).

Coding of smooth eye movements in three-dimensional space by frontal cortex

Kikuro Fukushima*, Takanobu Yamanobe*, Yasuhiro Shinmei*, Junko Fukushima*, Sergei Kurkin* & Barry W. Peterson†

** Department of Physiology, Hokkaido University School of Medicine, West 7, North 15, Sapporo 060-8638, Japan*
† Northwestern University Medical School, 303E Chicago Avenue, Chicago, Illinois 60611, USA

Through the development of a high-acuity fovea, primates with frontal eyes have acquired the ability to use binocular eye movements to track small objects moving in space[1]. The smooth-pursuit system moves both eyes in the same direction to track movement in the frontal plane (frontal pursuit), whereas the vergence system moves left and right eyes in opposite directions to track targets moving towards or away from the observer (vergence tracking). In the cerebral cortex and brainstem, signals related to vergence eye movements—and the retinal disparity and blur signals that elicit them—are coded independently of signals related to frontal pursuit[2–6]. Here we show that these types of signal are represented in a completely different way in the smooth-pursuit region of the frontal eye fields[7–11]. Neurons of the frontal eye field modulate strongly during both frontal pursuit and vergence tracking, which results in three-dimensional cartesian representations of eye movements. We propose that the brain creates this distinctly different intermediate representation to allow these neurons to function as part of a system that enables primates to track and manipulate objects moving in three-dimensional space.

In two monkeys, we recorded the activity of 225 neurons that was modulated during frontal pursuit and/or vergence tracking of laser spots projected onto a vertical or horizontal screen (Methods). Of 122 neurons tested during both frontal pursuit and vergence tracking, 80 (66%) responded to both (three-dimensional (3D) tracking). Thirty (25%) responded only during frontal pursuit and 12 (9%) responded only during vergence tracking.

Of the 92 neurons that responded during vergence tracking, 39 were activated during divergence (Fig. 1a), 45 during convergence (Fig. 3a, f) and 8 during both (data not shown). The neuron shown in Fig. 1a–d was activated strongly as the monkey tracked a target moving away from him (Fig. 1a) and more weakly during downward pursuit (Fig. 1d). Because the horizontal screen used to present targets moving in depth was at nose level, divergence eye movements were accompanied by small (0.8°) upward eye movements. This combined motion that was required during vergence tracking could not explain the increased discharge of this neuron during divergence, because it was activated during downward pursuit.

Similar arguments could be applied to the 36 neurons that had no response to vertical pursuit, or a response in the wrong direction, to account for their observed modulation during vergence tracking. For neurons whose vertical pursuit sensitivity was in the correct direction to contribute to their modulation during vergence tracking, the contribution was too small to account for the modulation observed during vergence tracking. Figure 2a shows this for a divergence plus upward pursuit neuron whose eye velocity sensitivity at 0.3, 0.5 and 1.0 Hz was much smaller during frontal pursuit than during vergence tracking.

Figure 2b plots the relationship between vergence-tracking and frontal-pursuit (combined horizontal, vertical) sensitivities for five groups of neurons. Sensitivities varied widely with a tendency for

convergence neurons (open squares) to have higher sensitivities to both vergence tracking and frontal pursuit. The lack of any clear correlation between sensitivities to vergence tracking and frontal pursuit suggested that these two inputs to frontal eye fields (FEFs) were independent. Figure 2c shows the spatial relationship between frontal-pursuit and vergence-tracking sensitivities. The radius indicates the ratio of frontal-pursuit sensitivity to vergence-tracking sensitivity so that neurons primarily sensitive to vergence tracking are near the centre. The angle is the preferred direction of frontal pursuit. As expected, most neurons had a ratio of less than one, and preferred directions were distributed widely, as has been reported previously for frontal pursuit[7–11].

FEF neurons could show an apparent sensitivity to 3D tracking if they were sensitive to the motion of a single eye, as has been observed in brainstem neurons[6]. To rule out this possibility, we recorded responses during vergence tracking of targets moving in the midsagittal plane or planes aligned with the left and right eyes. None of the neurons that had vertical or oblique preferred directions showed a clear monocular preference (Fig. 1a–c)—modulation was similar regardless of whether the net vergence movement was produced by motion of the left, right or both eyes. Rate–velocity relationships for target movements in the three planes were also similar (Fig. 2a), again suggesting that none of these neurons had a monocular preference.

Summation also accounted for the behaviour of neurons that responded to both vergence tracking and horizontal frontal pursuit. Figure 3a and b shows the normalized discharge modulations (mean ± s.e.m.) of 10 neurons whose discharge increased during convergence and leftward pursuit (Fig. 3a, black and red lines, respectively). When the target moved in the left-eye-aligned plane, convergent movements of the right eye were accompanied by leftward frontal pursuit, and the discharge modulation during this condition (Fig. 3b, black) was predicted well by the linear addition of modulations related to vergence and horizontal tracking (Fig. 3b, blue) derived from data in Fig. 3a.

We made a similar comparison for 20 neurons that responded strongly to horizontal pursuit (the above 10 convergence plus leftward pursuit neurons, 5 convergence plus rightward pursuit neurons, 3 divergence plus leftward pursuit neurons, and 2 divergence plus rightward pursuit neurons). Figure 3c summarizes the comparison of actual and predicted modulations (gain and phase relative to target velocity) of the 20 neurons during one-eye-aligned conditions in which modulation was in the additive direction. For most neurons, actual modulations during one-eye-aligned conditions were predicted well by addition of the two components, and the correlation coefficients were high ($r > 0.8$) with linear regression slopes close to one. Similar summation was also seen in the subtractive direction when off-saturation at zero firing rate was taken into account (data not shown).

Visual association cortex neurons may be sensitive to both the velocity of motion in the frontal plane and the disparity of the target, which signals its position in depth[12–14]. During 3D sinusoidal target motion, such a neuron would discharge in phase with velocity of target motion in the frontal plane and with target position in depth. Most FEF neurons behaved differently. Modulation during 0.5-Hz frontal pursuit and vergence tracking was most closely related to velocity of target or eye motion (Figs 1a–c and 3a, d). Median phases (relative to velocity) of neurons that showed significant unidirectional responses were 10° lead and 1° lag during frontal pursuit and vergence tracking, respectively. Median sensitivities were 0.63 and 1.70 spikes s^{-1} per degree s^{-1}. Because modulations caused by frontal pursuit and vergence tracking add roughly linearly (Fig. 3a–c), we can show these sensitivities as 3D vectors in two views (Fig. 4a, b). Preferred directions are distributed widely in 3D space.

To check further that frontal-pursuit and vergence-tracking signals combine to produce enhanced tracking along oblique trajectories such as those shown in Fig. 4, we examined the activity of several neurons when the monkey tracked a virtual target (produced by dichoptic presentation of targets to right and left eyes in alternation using shutter glasses) that moved along a trajectory close to the predicted preferred oblique trajectory for that neuron. The normalized activity (mean ± s.e.m., Fig. 3e, black traces) of six neurons during pursuit along their expected optimal oblique directions was very close to the activity predicted (Fig. 3e, blue traces) by adding responses to the frontal-pursuit and vergence-tracking components of the trajectory (Fig. 3d). This indicates that it is indeed possible to predict a preferred direction of motion in 3D space from the component responses that we measured.

Recording locations in both monkeys were in the caudal part of the arcuate sulcus including the fundus and posterior bank, similar

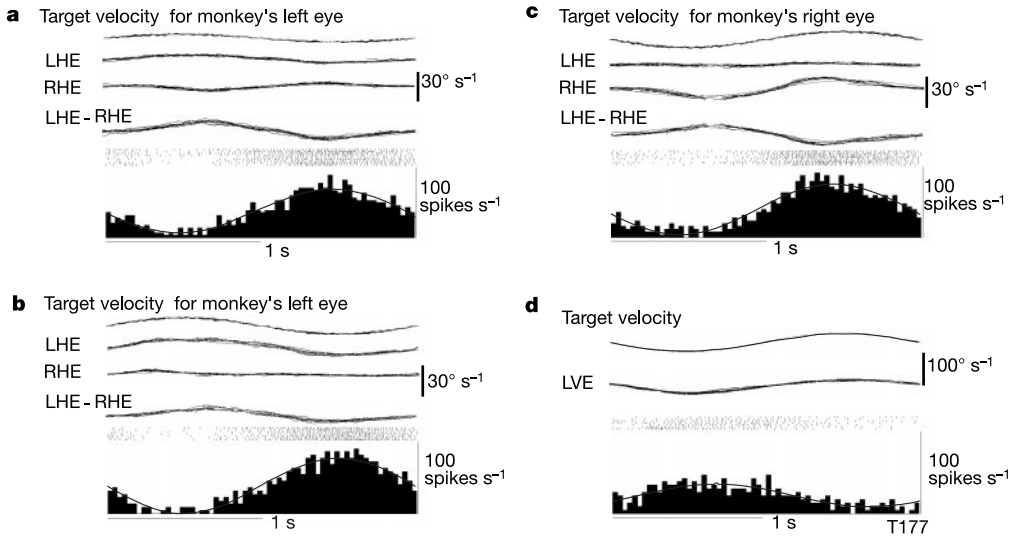

Figure 1 Representative activity of a pursuit neuron in the caudal frontal eye field. Response during target movement in the midsagittal (**a**), right-eye-aligned (**b**) and left-eye-aligned (**c**) planes and during vertical pursuit (**d**). LHE, left horizontal eye velocity; RHE, right horizontal eye velocity; LVE, left vertical eye velocity. Vergence velocity is indicated as LHE − RHE. Velocity calibration is 30° s^{-1} (**a**–**c**) and 100° s^{-1} (**d**).

to those observed in previous studies (Fig. 4c and refs 7–11). Neurons responding to frontal pursuit, vergence tracking or both were intermixed. Injection of the GABA (γ-amino butyric acid) agonist muscimol (10 μg in 1 μl of saline) at the site marked by an asterisk in Fig. 4c reduced the velocity of both frontal pursuit[15,16] and vergence tracking by about 50%, which supports our conclusion that both movements are controlled by the same FEF region. This result also suggests that the correlation of FEF neural activity with 3D tracking reflects that FEF has a role in generating 3D smooth eye movements.

FEF signals related to frontal pursuit and vergence tracking are similar in other ways. When a target that the monkey was tracking was blanked for 400–800 ms (refs 10, 11) during frontal pursuit and vergence tracking, both eye movement and neural discharge continued in the absence of visual input (Fig. 3f). Thus, as for frontal pursuit[10,11,17,18], discharge related to vergence tracking is not

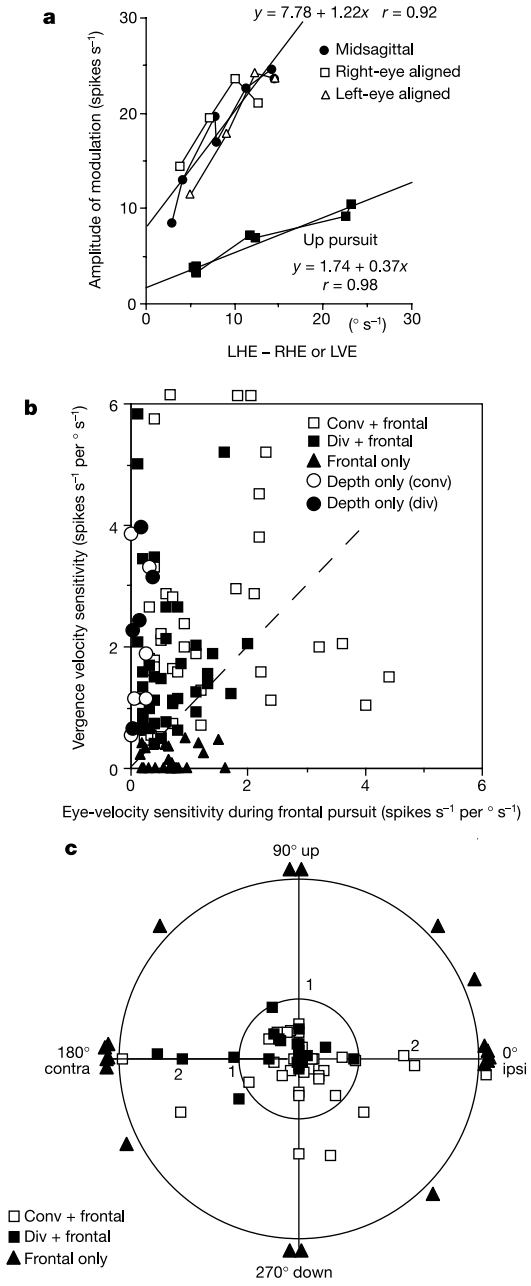

Figure 2 Eye velocity and vergence velocity sensitivity of caudal FEF neurons during frontal pursuit and vergence tracking. **a**, Discharge modulation of an up-pursuit plus divergence neuron plotted against vergence velocity for three target presentation conditions as indicated and vertical pursuit eye velocity with fitted linear regressions. LHE, left horizontal eye velocity; RHE, right horizontal eye velocity; LVE, left vertical eye velocity. **b**, Vergence-velocity sensitivity plotted against frontal-pursuit eye velocity sensitivity for the five indicated groups of neurons. The plot indicates some frontal-only and depth-only neurons with some eye and vergence velocity sensitivity, but harmonic distortion of their modulations were >100%. **c**, Ratio of frontal pursuit to vergence tracking eye-velocity sensitivity plotted against preferred directions for frontal pursuit for the indicated three groups of neurons. Symbols outside the plot frame in **b** and **c** exceeded the plotting scale. In **c**, ipsi and contra indicate ipsilateral and contralateral to the recording side.

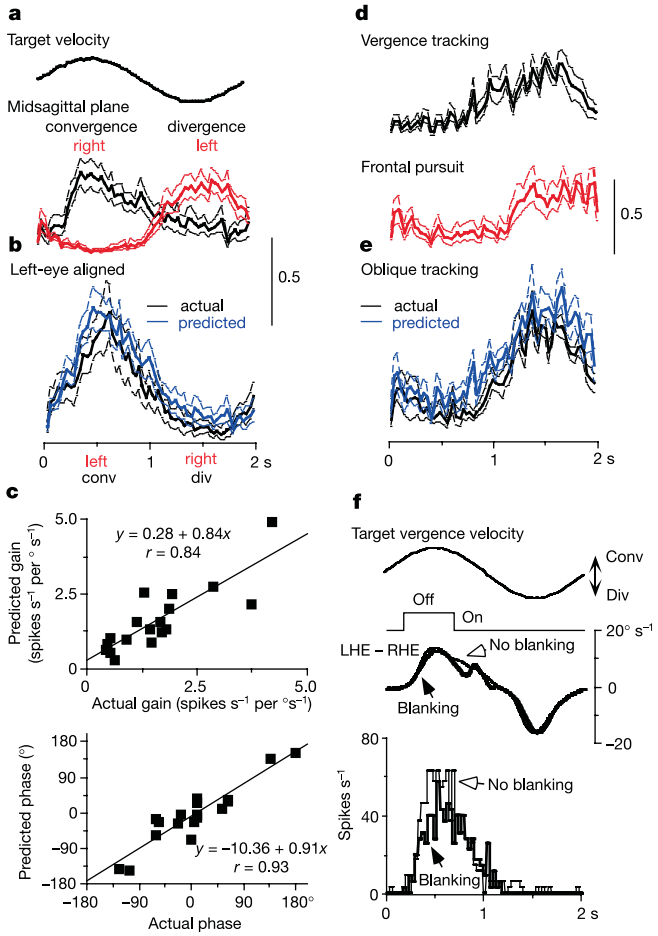

Figure 3 Linear summation of frontal pursuit and vergence tracking responses and maintenance of discharge during target blanking. **a**, **b**, Normalized discharge modulations (mean ± s.e.m.) during left-eye-aligned conditions for 10 convergent plus leftward pursuit neurons (**b**, actual) compared with predicted modulation (**b**, predicted) computed by adding modulations during midsagittal vergence tracking (**a**, black) and frontal pursuit (**a**, red). **c**, Comparison of actual and predicted modulations (gain and phase relative to target velocity) of 20 neurons with vergence plus horizontal pursuit sensitivities during one-eye-aligned conditions with fitted linear regressions. **d**, **e**, Normalized discharge modulations (mean ± s.e.m.) of six neurons during midsagittal vergence tracking (**d**, black), frontal pursuit (**d**, red) and when the monkey tracked a virtual target that moved along the expected optimal oblique directions for those neurons (**e**, black). Oblique target motion was presented by dichoptic spot stimulus for each eye. Predicted discharge modulation (**e**, predicted) was computed by adding modulations during vergence tracking and frontal pursuit (**d**). **f**, Eye movement and discharge of FEF neuron in vergence tracking cycles with (thick line) and without (thin line) target blanking. Note that tracking changes from the divergence direction to convergence in the absence of retinal input and that convergence-related activity of this neuron is identical on blanking and control trials until 300 ms into the blanking period. Afterwards activity during blanking is reduced and later still corrections occur after vision is restored.

dependent on retinal input. For vergence tracking, this also serves as a control that shows that responses do not simply reflect retinal disparity of a target.

The vergence and smooth-pursuit systems are considered to have separate neural substrates, as suggested more than a century ago[1,19,20]. But 66% of our FEF neurons were sensitive to both frontal pursuit and vergence tracking. In the brainstem, vergence-related (not 3D) neurons located around the oculomotor nucleus project to the medial rectus subdivision and provide a vergence signal to these motoneurons[1,4,5,21]. Neurons have also been reported whose discharge selectively reflects movement of one eye[6], which may reflect precisely matched sensitivities to both frontal pursuit and vergence tracking. How could 3D motion signals in the FEF with their wide range of sensitivities be converted into commands to control the version and vergence motions of the two eyes? This could be accomplished by taking a weighted sum of the activity of neurons with different combinations of vergence and version activity. For example, consider a set of four neurons that respond with equal sensitivity to both frontal pursuit and vergence tracking, with D, C, L and R indicating, respectively, activation during tracking in divergence, convergence, leftward and rightward directions (so that, for example, CL indicates a neuron that is activated equally during convergence and leftward tracking). The combination CL + CR − DL − DR will yield a net convergence (+)/divergence (−) signal. This could provide input to cortical[2,5] or brainstem[4,20] circuits that selectively control vergence and accommodation. CR + DR − CL − DL would provide a pure version signal. The combinations CR − DL and CL − DR yield monocular signals that are appropriate to drive the right and left eyes[6]. Selection of appropriate weights would allow such signals to be extracted from any set of neurons with a broad array of 3D preferred directions.

Because FEF discharge related to frontal pursuit and vergence tracking persists during target blanking, it is not dependent on sensory input but instead has a substantial motor or predictive component. Ultimately, however, the discharge and related eye movement are guided by visual input. It is interesting that 3D motion velocity signals have not yet been found in the visual system. Disparity-related signals reported in visual motion areas medial temporal (MT) and medial superior temporal (MST) cortices are mostly static depth position signals[12,14] and discharge of MST neurons related to vergence velocity has been reported only in response to motion of large fields of dots[22]. Signals related to 3D

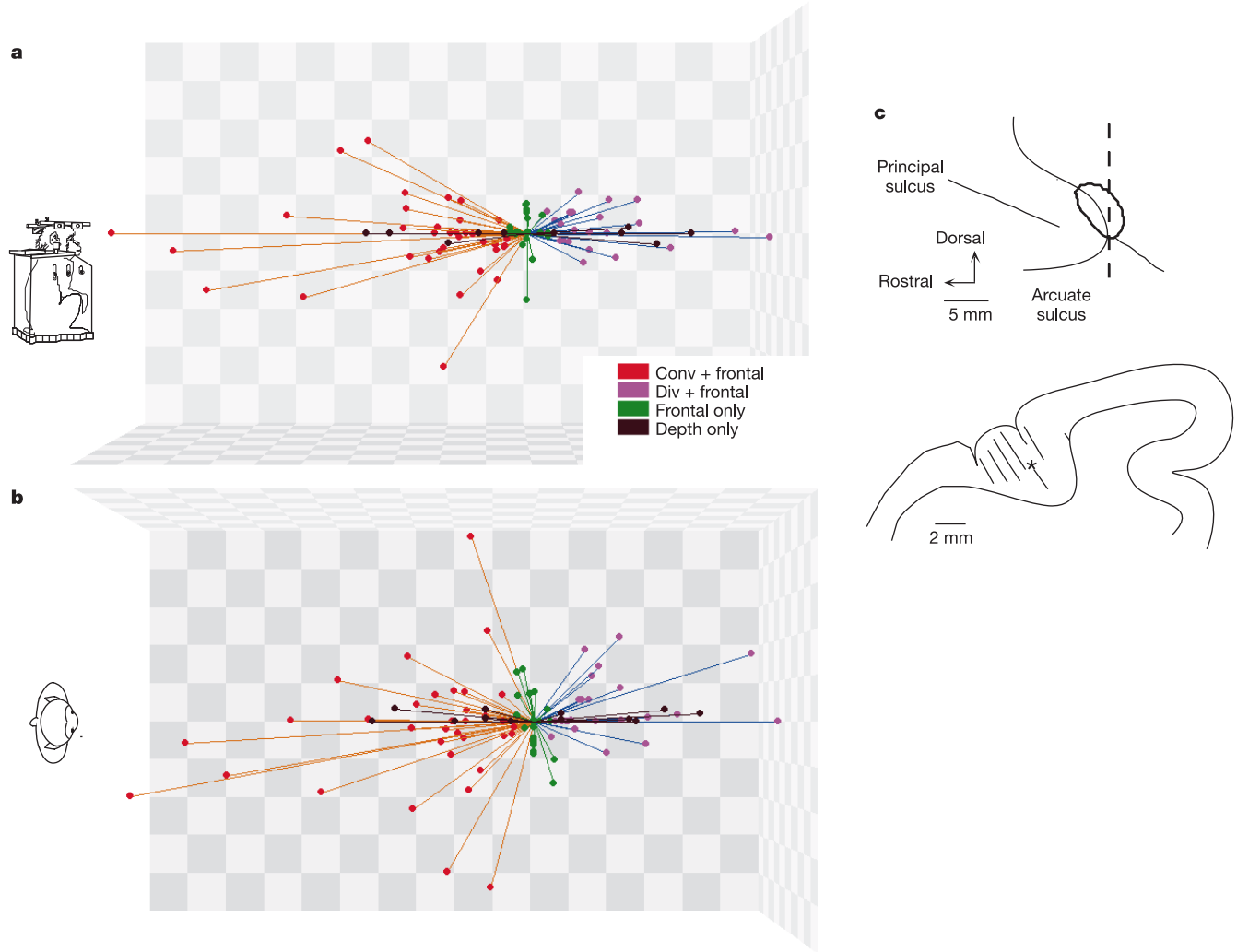

Figure 4 Three-dimensional sensitivity vectors of caudal FEF neurons and recording locations. **a**, **b**, 3D representation of preferred tracking directions and magnitudes of discharge sensitivity for the four indicated groups of FEF neurons (dots with lines). Three-dimensional sensitivity vectors were calculated for each neuron by assuming that frontal pursuit and vergence tracking sum linearly, and each direction was drawn to originate from a single point along the monkey's straight-ahead gaze. **c**, Recording locations in monkey 1. The area indicated by the thick line in the top view of arcuate sulcus region indicates entry points of tracks in which neurons related to frontal pursuit and vergence tracking were observed. A cross-section through the area indicated by a dashed line shows trajectory of tracks containing such responsive neurons, which were typically encountered at depths of 3–5 mm from the surface.

target motion have been reported in the ventral intraparietal (VIP) area[23], but the activity depends on where the target trajectory will intersect the body, which suggests that position signals are also critical there. These findings underscore the uniqueness of the 3D motion velocity signals in FEF.

Thus, our data indicate that the brain creates an intermediate representation of tracking eye movements that are distinctly different from those reported in other sensory and motor areas of the brain. We propose that this occurred in response to an important factor driving primate evolution—the need to coordinate eye and hand movements to track and manipulate objects in a 3D world. By creating an intermediate representation of eye movements in a 3D coordinate frame that resembles the one in which we perceive the world, the brain opens the way for facile coordination of oculomotor signals with somatomotor signals coded in similar extrinsic frames. We predict that neighbouring frontal lobe areas will show related coding schemes for many different movements. Neurons in adjacent regions of FEF that control small saccades have disparity-tuned visual responses[24], which suggests that part of the saccadic FEF also uses a 3D coordinate frame. Conversely, largely separate coding of version and vergence movements in more rostral areas of FEF and area 8 has been reported (ref. 2). Perhaps these form part of a gaze-orienting system in which independent control of version and vergence is advantageous.

Recordings in the caudal ventral premotor cortex (area F4), which is located posterior to the smooth-pursuit area of FEF, have revealed neurons that code hand movements in a 3D extrinsic coordinate frame that is referred to the current centre of gaze[25]. F4 neurons also exhibit sensory responses that reflect the 3D location of a visual target with respect to a point on the body surface[26–29]. These signals could be readily derived by combining 3D eye and hand movement signals, whereas they would be more difficult to compute from signals intrinsic to each system such as version/vergence or joint-angle signals. □

Methods

Animals

Two monkeys (*Macaca fuscata*, 4.5 and 6.0 kg) were used in the experiments. We carried out all procedures in strict compliance with the Guide for the Care and Use of Laboratory Animals (DHEW Publication NIH85-23, 1985). Specific protocols were approved by the Animal Care and Use Committee of Hokkaido University School of Medicine. Methods for animal preparation, training and recording were similar to previous studies[10,11] except for binocular recording and vergence task conditions, and are summarized here only briefly.

Animal preparation and training

A scleral search coil was implanted on each eye to record vertical and horizontal components of eye movement for both eyes. Monkeys' heads were restrained in the stereotaxic plane in a primate chair. Animals were trained to track a 0.2° laser spot backprojected onto a vertical screen 75 cm in front of the monkey's eyes for a reward of apple juice. A second horizontal screen was positioned at the level of the monkey's nose to project another 2 mm diameter laser spot from above. This screen was tilted 10° downward towards the front. From the monkey's viewpoint, the spot moved sinusoidally (0.3–1.0 Hz) from 28 to 70 cm in front of his eyes within the midsagittal, right- or left-eye-aligned plane. Accurate tracking of the midsagittal target required 1.3° movements of each eye, whereas tracking of right- or left-eye-aligned targets required 2.6° movement of the opposite eye. Because of the placement of the horizontal screen, vergence eye movements were accompanied by 0.8° vertical pursuit. A virtual target spot was presented on a computer monitor to test response of some neurons during 3D oblique tracking. For this, we used a time-multiplexed display with liquid crystal shutters synchronized to the alternating images for each eye at a refresh rate of 120 Hz.

Recordings

Extracellular recordings were made in the peri-arcuate sulcus region. Once an isolated neuron responding during frontal-pursuit or vergence tracking was encountered, the monkey was assigned vergence tracking tasks (Fig. 1a–c) followed by frontal-pursuit tasks using the vertical screen with a target moving at 0.5 Hz (5–10°) in different directions to determine the preferred direction for activation. We also tested frontal pursuit at smaller amplitudes (0.5–3.0°) for many neurons to confirm that neuronal discharge was related linearly to velocity of tracking.

Data collection and processing

As described previously[11], eye, target and chair position signals and their derivatives were low-pass filtered (250 Hz) and digitized at 500 Hz. Neural discharge was discriminated and stored in temporal register with analog signals. Data segments containing saccades were identified by an interactive computer program and ignored in the following analysis. We constructed cycle histograms by averaging the discharge of each neuron over 10–30 cycles. Sinusoids were fit by least squares to neuron and eye movement responses. The signal-to-noise ratio of the response was defined as the ratio of amplitude of the fitted fundamental frequency component to the root mean-square amplitude of the third to the eighth harmonics. Harmonic distortion was defined as the ratio of the amplitude of the second harmonic to that of the fundamental. Responses with harmonic distortion >50% or signal to noise ratio <1.0 were discarded. Phase shifts were measured between the peak of the fundamental component of the response and the peak stimulus velocity. Phases of neural discharge relative to version or vergence eye-velocity were then calculated by subtraction.

We estimated preferred direction of individual neuron response during pursuit using a gaussian function as described[10,11,30]. Each neuron's eye-velocity sensitivity during vergence tracking and frontal pursuit at 0.5 Hz was calculated by dividing the amplitude of the fundamental component of discharge modulation either by the amplitude of vergence tracking velocity or by the amplitude of eye-velocity modulation along the preferred frontal-pursuit direction. For neurons that had vertical pursuit sensitivity, we subtracted the modulation estimated to be due to the vertical component of eye movement from the discharge modulation during vergence tracking. (We chose sensitivity with respect to eye movement rather than sensitivity with respect to 'linear excursion of the target' in external space because we were relating FEF activity to eye movement. Choosing linear excursion would reduce the 2.7:1 sensitivity ratio in favour of vergence tracking that was described above by a factor of 6, resulting in a 0.44:1 sensitivity ratio in regard to target excursion.)

We normalized discharge modulations relative to maximal discharge rate during midsagittal vergence tracking and frontal pursuit for each neuron. Discharge modulations during one-eye-aligned conditions and 3D oblique tracking using a virtual display were also normalized relative to this maximal rate for each neuron. Normalized modulations were then averaged for many neurons to obtain population response.

To examine whether higher vergence-velocity sensitivity of many neurons was due to the effects of different target size (larger for convergence, smaller for divergence), we compared pursuit response using the vertical screen with a target of two different sizes (0.2° and 0.6° in diameter) comparable to the target sizes from the monkey's viewpoint at farthest and nearest distance on the horizontal screen. We also compared pursuit response to the target moving horizontally on the horizontal screen at the nearest and farthest positions. None of these conditions provided evidence that pursuit responses depended on target size or distance. Recording locations were histologically confirmed by making electrolytic lesions through the recording electrodes as described[10,11].

Received 26 April; accepted 13 June 2002; doi:10.1038/nature00953.

1. Leigh, R. & Zee, D. S. *The Neurology of Eye Movements* (Oxford Univ. Press, New York, 1999).
2. Gamlin, P. D. & Yoon, K. An area for vergence eye movement in primate frontal cortex. *Nature* **407,** 1003–1007 (2000).
3. Cumming, B. in *Visual Detection of Motion* (eds Smith, A. T. & Snowdon, R. J.) 333–366 (Academic, London, 1994).
4. Mays, L. E., Porter, J. D., Gamlin, P. D. R. & Tellow, C. A. Neural control of vergence eye movements: neurons encoding vergence velocity. *J. Neurophysiol.* **56,** 1007–1021 (1986).
5. Mays, L. E. & Gamlin, P. D. Neuronal circuitry controlling the near response. *Curr. Opin. Neurobiol.* **5,** 763–768 (1995).
6. Zhou, W. & King, W. M. Premotor commands encode monocular eye movements. *Nature* **393,** 692–695 (1998).
7. MacAvoy, M. G., Gottlieb, J. P. & Bruce, C. J. Smooth pursuit eye movement representation in the primate frontal eye field. *Cereb. Cortex* **1,** 95–102 (1991).
8. Gottlieb, J. P., MacAvoy, M. G. & Bruce, C. J. Neural responses related to smooth pursuit eye movements and their correspondence with electrically elicited slow eye movements in the primate frontal eye field. *J. Neurophysiol.* **72,** 1634–1653 (1994).
9. Tian, J. & Lynch, J. C. Functionally defined smooth and saccadic eye movement subregions in the frontal eye field of Cebus monkeys. *J. Neurophysiol.* **76,** 2740–2771 (1996).
10. Tanaka, K. & Fukushima, K. Neuronal responses related to smooth pursuit eye movements in the periarcuate cortical area of monkeys. *J. Neurophysiol.* **80,** 28–47 (1998).
11. Fukushima, K., Sato, T., Fukushima, J., Shinmei, Y. & Kaneko, C. R. S. Activity of smooth pursuit-related neurons in the monkey periarcuate cortex during pursuit and passive whole body rotation. *J. Neurophysiol.* **83,** 563–587 (2000).
12. Maunsell, J. H. & van Essen, D. C. Functional properties of neurons in middle temporal visual area of the macaque monkey. II. Binocular interactions and sensitivity to binocular disparity. *J. Neurophysiol.* **49,** 1148–1167 (1983).
13. Roy, J. P., Komatsu, H. & Wurtz, R. H. Disparity sensitivity of neurons in monkey extrastriate area MST. *J. Neurosci.* **12,** 2478–2492 (1992).
14. Eifuku, S. & Wurtz, R. H. Response to motion in extrastriate area MSTl: disparity sensitivity. *J. Neurophysiol.* **82,** 2462–2475 (1999).
15. Shi, D., Friedman, H. R. & Bruce, C. J. Deficits in smooth pursuit eye movements after muscimol inactivation within the primate frontal eye field. *J. Neurophysiol.* **80,** 458–464 (1998).
16. Fukushima, K., Sato, T. & Fukushima, J. Vestibular-pursuit interactions: gaze-velocity and target-velocity signals in the monkey frontal eye fields. *Ann. NY Acad. Sci.* **871,** 248–259 (1999).
17. Ferrera, V. P. & Barborica, A. Predictive responses to invisible target motion in macaque frontal eye field. *Soc. Neurosci. Abstr.* **26,** 669 (2000).
18. Fukushima, K., Yamanobe, T., Shinmei, Y. & Fukushima, J. Predictive responses of peri-arcuate pursuit neurons to visual target motion. *Exp. Brain Res.* **145,** 104–120 (2002).
19. Semmlow, J. L., Weihong, Y. & Alvarez, T. L. Evidence for separate control of slow version and vergence eye movements: support for Hering's law. *Vision Res.* **38,** 1145–1152 (1998).
20. Gamlin, P. D. Subcortical neural circuits for ocular accommodation and vergence in primates. *Ophthal. Physiol. Opt.* **2,** 81–89 (1999).
21. Judge, S. J. & Cumming, B. G. Neurons in the monkey midbrain with activity related to vergence eye movements and accommodation. *J. Neurophysiol.* **55,** 915–930 (1986).

22. Takemura, A., Inoue, Y., Kawano, K., Quaia, C. & Miles, F. A. Single-unit activity in cortical area MST associated with disparity-vergence eye movements: evidence for population coding. *J. Neurophysiol.* **85,** 2245–2266 (2001).
23. Colby, C. L., Duhamel, J. R. & Goldberg, M. E. Ventral intraparietal area of the macaque: anatomic location and visual response properties. *J. Neurophysiol.* **69,** 902–914 (1993).
24. Ferraina, S., Pare, M. & Wurtz, R. H. Disparity sensitivity of frontal eye field neurons. *J. Neurophysiol.* **83,** 625–629 (2000).
25. Kakei, S., Hoffman, D. S. & Strick, P. L. Direction of action is represented in the ventral premotor cortex. *Nature Neurosci.* **4,** 1020–1025 (2001).
26. Mushiake, H., Tanatsugu, Y. & Tanji, J. Neuronal activity in the ventral part of premotor cortex during target-reach movement is modulated by direction of gaze. *J. Neurophysiol.* **78,** 567–571 (1997).
27. Fogassi, L. *et al.* Space coding by premotor cortex. *Exp. Brain Res.* **89,** 686–690 (1992).
28. Fogassi, L. *et al.* Coding of peripersonal space in inferior premotor cortex (area F4). *J. Neurophysiol.* **76,** 141–157 (1996).
29. Graziano, M. S., Hu, X. T. & Gross, C. G. Visuospatial properties of ventral premotor cortex. *J. Neurophysiol.* **77,** 2268–2292 (1997).
30. Krauzlis, R. J. & Lisberger, S. G. Directional organization of eye movement and visual signals in the floccular lobe of the monkey cerebellum. *Exp. Brain Res.* **109,** 289–302 (1996).

Acknowledgements

We thank B. Cumming, M. Goldberg, S. Lisberger, F. Miles and P. Strick for comments on the manuscript, and T. Akao and F. Sato for participation in some experiments. This work was supported in part by CREST of JST, Japanese Ministry of Education, Science, Culture and Sports, and Marna Cosmetics.

Competing interests statement

The authors declare that they have no competing financial interests.

Correspondence and requests for materials should be addressed to K.F. (e-mail: kikuro@med.hokudai.ac.jp).

Loss of the Lkb1 tumour suppressor provokes intestinal polyposis but resistance to transformation

Nabeel Bardeesy*, Manisha Sinha*, Aram F. Hezel*, Sabina Signoretti†, Nathaniel A. Hathaway*, Norman E. Sharpless*, Massimo Loda†, Daniel R. Carrasco† & Ronald A. DePinho*

** Department of Adult Oncology, Dana-Farber Cancer Institute and Departments of Medicine and Genetics, Harvard Medical School, Boston, Massachusetts 02115, USA*

† Department of Pathology, Brigham and Women's Hospital, Harvard Medical School, Boston, Massachusetts 02115 USA

Germline mutations in *LKB1* (also known as *STK11*) are associated with Peutz–Jeghers syndrome (PJS), a disorder with predisposition to gastrointestinal polyposis and cancer[1]. PJS polyps are unusual neoplasms characterized by marked epithelial and stromal overgrowth but have limited malignant potential[2]. Here we show that *Lkb1*$^{+/-}$ mice develop intestinal polyps identical to those seen in individuals affected with PJS. Consistent with this *in vivo* tumour suppressor function, Lkb1 deficiency prevents culture-induced senescence without loss of *Ink4a/Arf* or *p53*. Despite compromised mortality, *Lkb1*$^{-/-}$ mouse embryonic fibroblasts show resistance to transformation by activated Ha-*Ras* either alone or with immortalizing oncogenes. This phenotype is in agreement with the paucity of mutations in *Ras* seen in PJS polyps[3,4] and suggests that loss of Lkb1 function as an early neoplastic event renders cells resistant to subsequent oncogene-induced transformation. In addition, the Lkb1 transcriptome shows modulation of factors linked to angiogenesis, extracellular matrix remodelling, cell adhesion and inhibition of *Ras* transformation. Together, our data rationalize several features of PJS polyposis—notably its peculiar histopathological presentation and limited malignant potential—and place Lkb1 in a distinct class of tumour suppressors.

Compared with other hereditary tumour syndromes, PJS has several unusual features. Although germline mutations in *LKB1* are associated with a cancer-prone condition[1,5], the *LKB1* gene is very rarely mutated or epigenetically silenced in sporadic tumours[6–8]. Heterozygosity for PJS is characterized by gastrointestinal polyps, but these polyps (hamartomas) possess low malignant potential and comprise disorganized non-dysplastic gastrointestinal mucosa with prominent branching smooth muscle components[2]. In addition, although gastrointestinal carcinomas develop with increased frequency in individuals with PJS, it is not clear whether hamartomas are precursor lesions of these carcinomas[2].

To investigate these paradoxical features of PJS, we generated mice carrying a conditional *Lkb1* allele (Fig. 1a, b). Mice carrying either one copy of the null allele (*Lkb1*$^{-}$) or a functional, floxed allele deleted for the *neomycin* resistance (*neo*^{r}) gene (*Lkb1*^{lox}) were generated in crosses with *EIIa–Cre*[9] or *CAGG–Flpe*[10] transgenic strains, respectively. Molecular analyses showed the expected recombinant alleles and absence of Lkb1 protein in mouse embryonic fibroblasts (MEFs) after Cre-mediated excision (Fig. 1c–e and see below). *Lkb1*$^{+/-}$ and *Lkb1*$^{lox/+}$ offspring were born at expected mendelian frequencies and showed no gross abnormalities. Consistent with previous results[11], *Lkb1*$^{-/-}$ mice had a lethal condition that manifested at about embryonic day (E) 8.5–11, with defects in vasculogenesis and placental development (data not shown).

We studied the tumour predisposition of these mice and found that 40 of 59 *Lkb1*$^{+/-}$ and 0 of 65 wild-type mice presented with symptoms of gastrointestinal obstruction at an average age of 43 weeks (Fig. 2a). Autopsy of symptomatic *Lkb1*$^{+/-}$ mice showed that polyps (between 1 and >15) were present throughout the gastrointestinal tract (Fig. 2b, c, and Supplementary Information Fig. 1), presenting as mucosal hamartomas with histological features mirroring those encountered in individuals with PJS or juvenile polyposis[2]. Detailed histopathological analysis failed to discern dysplastic or adenomatous changes in 15 polyps examined, and none of the polyps showed mutations in Ki-*ras* (Methods). A single *Lkb1*$^{+/-}$ mouse presented with a benign serous cystadenoma of the pancreas and two *Lkb1*$^{+/-}$ mice showed asymptomatic, benign uterine epithelial tumours (data not shown), but otherwise an extensive histological survey of 20 *Lkb1*$^{+/-}$ mice failed to identify additional neoplasms in other organs or abnormal mucocutaneous pigmentation up to an age of 45 weeks.

Hamartomas in individuals with PJS show loss of the wild-type *LKB1* allele in the epithelial compartment[3,4,12]. Correspondingly, laser capture microdissection (LCM) and allele-specific polymerase

Table 1 **Analysis of Lkb1 in polyps**

Tumour no.	LCM*	IHC*
1	Loss	Negative
2	Loss	Negative
3	Retention	Positive
4	Retention	Negative
5	Loss	ND
6	Retention	Negative
7	Retention	Negative
8	Retention	Positive
9	Retention	Positive
10	Retention	Positive
12	Retention	ND
13	Retention	Negative
14	ND	Negative
15	ND	Positive
16	ND	Negative
17	ND	Positive
Total	3/12	8/14

*Retention/loss denotes status of wild-type *Lkb1* allele. IHC, immunohistochemistry using an antibody against Lkb1; LCM, laser capture microdissection; ND, not determined or not informative.

